Metamagnetics with rainbow colors

Wenshan Cai, Uday K. Chettiar, Hsiao-Kuan Yuan, Vashista C. de Silva, Alexander V. Kildishev, Vladimir P. Drachev, and Vladimir M. Shalaev

School of Electrical and Computer Engineering and Birck Nanotechnology Center, Purdue University, West Lafayette, Indiana 47907, USA
shalaev@purdue.edu

Abstract: A family of coupled nanostrips with varying dimensions is demonstrated exhibiting optical magnetic responses across the whole visible spectrum, from red to blue. We refer to such a phenomenon as rainbow magnetism. The experimental and analytical studies of such structures provide us with a universal building block and a general recipe for producing controllable optical magnetism for various practical implementations.

OCIS codes: (160.4670) Optical material; (160.4760) Optical properties; (260.5740) Resonance; (310.6860) Thin films, optical properties.

References and links

1. J. B. Pendry, A. J. Holden, D. J. Robbins, and W. J. Stewart, "Magnetism from conductors and enhanced nonlinear phenomena," IEEE Trans. Microwave Theory Tech. **47**, 2075 (1999).
2. D. R. Smith, W. J. Padilla, D. C. Vier, S. C. Nemat-Nasser, and S. Schultz, "Composite medium with simultaneously negative permeability and permittivity," Phys. Rev. Lett. **84**, 4184 (2000).
3. T. J. Yen, W. J. Padilla, N. Fang, D. C. Vier, D. R. Smith, J. B. Pendry, D. N. Basov, and X. Zhang, "Terahertz magnetic response from artificial materials," Science **303**, 1494 (2004).
4. S. Linden, C. Enkrich, M. Wegener, J. Zhou, T. Koschny, and C. M. Soukoulis, "Magnetic response of metamaterials at 100 Terahertz," Science **306**, 1351 (2004).
5. S. Zhang, W. Fan, B. K. Minhas, A. Frauenglass, K. J. Malloy, and S. R. J. Brueck, "Midinfrared resonant magnetic nanostructures exhibiting a negative permeability," Phys. Rev. Lett. **94**, 037402 (2005).
6. T. F. Gundogdu, I. Tsiapa, A. Kostopoulos, G. Konstantinidis, N. Katsarakis, R. S. Penciu, M. Kafesaki, E. N. Economou, Th. Koschny, and C. M. Soukoulis, "Experimental demonstration of negative magnetic permeability in the far-infrared frequency regime," Appl. Phys. Lett. **89**, 084103 (2006).
7. C. Enkrich, M. Wegener, S. Linden, S. Burger, L. Zschiedrich, F. Schmidt, J. F. Zhou, Th. Koschny, and C. M. Soukoulis, "Magnetic metamaterials at telecommunication and Visible frequencies," Phys. Rev. Lett. **95**, 203901 (2005).
8. V. A. Podolskiy, A. K. Sarychev, and V. M. Shalaev, "Plasmon modes in metal nanowires and left-handed materials," J. Nonlinear Opt. Phys. Mater. **11**, 65 (2002).
9. A. V. Kildishev, W. Cai, U. K. Chettiar, H.-K. Yuan, A. K. Sarychev, V. P. Drachev, and V. M. Shalaev, "Negative refractive index in optics of metal-dielectric composites," J. Opt. Soc. Am. B **23**, 423 (2006).
10. G. Shvets and Y. A. Urzhumov, "Negative index meta-materials based on two-dimensional metallic structures," J. Opt. A **8**, S122 (2006).
11. U. K. Chettiar, A. V. Kildishev, T. A. Klar, and V. M. Shalaev, "Negative index metamaterial combining magnetic resonators with metal films," Opt. Express **14**, 7872 (2006).
12. J. Zhou, Th. Koschny, M. Kafesaki, E. N. Economou, J. B. Pendry, and C. M. Soukoulis, "Saturation of the magnetic response of split-ring resonators at optical frequencies," Phys. Rev. Lett. **95**, 223902 (2005).
13. M. W. Klein, C. Enkrich, M. Wegener, C. M. Soukoulis, and S. Linden, "Single-slit split-ring resonators at optical frequencies: limits of size scaling," Opt. Lett. **31**, 1259 (2006).
14. H.-K. Yuan, U. K. Chettiar, W. Cai, A. V. Kildishev, A. Boltasseva, V. P. Drachev, and V. M. Shalaev, "A negative permeability material at red light," Opt. Express **15**, 1078 (2007).
15. V. M. Shalaev, W. Cai, U. K. Chettiar, H.-K. Yuan, A. K. Sarychev, V. P. Drachev, and A. V. Kildishev, "Negative index of refraction in optical metamaterials," Opt. Lett. **30**, 3356 (2005).
16. S. Zhang, W. Fan, N. C. Panoiu, K. J. Malloy, R. M. Osgood, and S. R. J. Brueck, "Experimental demonstration of near-infrared negative-index metamaterials," Phys. Rev. Lett. **95**, 137404 (2005).
17. G. Dolling, C. Enkrich, M. Wegener, C. M. Soukoulis, and S. Linden, "Low-loss negative-index metamaterial at telecommunication wavelengths," Opt. Lett. **31**, 1800 (2006).
18. P. A. Belov and C. R. Simovski, "Subwavelength metallic waveguides loaded by uniaxial resonant scatterers," Phys. Rev. E **72**, 036618 (2005).

#80062 - $15.00 USD Received 13 February 2007; accepted 27 February 2007

19. A. Ourir, A. de Lustrac, and J.-M. Lourtioz, "All-metamaterial-based subwavelength cavities (λ/60) for ultrathin directive antennas," Appl. Phys. Lett. **88**, 084103 (2006).
20. V. A., Fedotov, P. L. Mladyonov, S. L. Prosvirnin, and N. I. Zheludev, "Planar electromagnetic metamaterial with a fish scale structure," Phys. Rev. E **72**, 056613 (2005).
21. B. T. Schwartz and R. Piestun, "Total external reflection from metamaterials with ultralow refractive index," J. Opt. Soc. Am. B **20**, 2448 (2003).
22. J. B. Pendry, D. Schurig, and D. R. Smith, "Controlling electromagnetic fields," Science **312**, 1780 (2006).
23. D. Schurig, J. J. Mock, B. J. Justice, S. A. Cummer, J. B. Pendry, A. F. Starr, and D. R. Smith, "Metamaterial electromagnetic cloak at microwave frequencies," Science **314**, 977 (2006).
24. I. Puscasu, W. L. Schaich, and G. D. Boreman, "Modeling parameters for the spectral behavior of infrared frequency-selective surfaces," Appl. Opt. **40**, 118 (2001).
25. R. W. Wood, "Anomalous diffractive gratings," Phys. Rev. **48**, 928 (1935).
26. P. B. Johnson and R. W. Christy, "Optical constants of the noble metals," Phys. Rev. B **6**, 4370 (1972).
27. T. Koschny, P. Markoŝ, D. R. Smith, and C. M. Soukoulis, "Resonant and antiresonant frequency dependence of the effective parameters of metamaterials," Phys. Rev. E **68**, 065602(R) (2003).
28. V. Lomakin, Y. Fainman, Y. Urzhumov, and G. Shvets, "Doubly negative metamaterials in the near infrared and visible regimes based on thin film nanocomposites," Opt. Express **14**, 11164 (2006).
29. J. Zhou, L. Zhang, G. Tuttle, T. Koschny, and C. M. Soukoulis, "Negative index materials using simple short wire pairs," Phys. Rev. B **73**, 041101(R) (2006).
30. D. R. Smith, S. Schultz, P. Markoš, and C. M. Soukoulis, "Determination of effective permittivity and permeability of metamaterials from reflection and transmission coefficients," Phys. Rev. B **65**, 195104 (2002).

1. Introduction

In optics, the magnetic response (susceptibility) of most natural materials is very small in comparison to the dielectric susceptibility, thus limiting the interaction of atoms mainly to the electric component of light and leaving the magnetic component largely unexploited. Metamaterials can fundamentally change light-matter interaction by making light "ambidextrous" in the optical range, with its magnetic and electric components playing equally important roles. In the past few years, split-ring resonators [1] (SRRs) and their analogues have been the magnetic "meta-atoms" of choice, and their magnetic response has spanned several decades of the electromagnetic spectrum from C-band microwave frequencies up to the optical wavelength of 800 nm [2-7]. At visible wavelengths, however, other structures like coupled nanorods [8] or nanostrips [9-11] are preferred because there are intrinsic limits to scaling SRR sizes in order to exhibit a magnetic response in the optical range [12,13].

Here we study the general resonant properties of magnetic metamaterials consisting of arrays of paired thin silver strips. The magnetism in such a structure has been discussed theoretically [9, 10] and was recently demonstrated experimentally at the very red end of the visible range [14]. However it remained a challenging task to "upgrade" magnetic structures to shorter wavelengths due to both design and fabrication difficulties. Here we demonstrate structures with magnetic responses across the whole visible spectrum by creating a family of paired-strip samples with varying geometries. The dependence of the magnetic resonance wavelength on the geometric parameters is studied both experimentally and theoretically. We note that any controllable optical magnetic responses, whether they have a positive or negative permeability, are important for various implementations such as negative refraction [15-17], subwavelength waveguides and antennas [18,19], spectral selective filters [20], total external reflection [21], and electromagnetic cloaking devices [22,23].

2. Sample descriptions

Figure 1(a) shows a cross-sectional schematic of the coupled nanostrip samples. A pair of thin silver strips with thickness t is separated by an alumina spacer with thickness d and refractive index n_d. The whole sandwich stack is trapezoidally shaped with an average width of w and a bottom width of w_b due to fabrication limitations. The thickness of each silver layer and the alumina spacer are t = 35 nm and d = 40 nm, respectively. These parameters are optimized values based on spatial harmonic analysis. For different samples, we vary the width w of the

#80062 - $15.00 USD Received 13 February 2007; accepted 27 February 2007

strips to obtain optical magnetic resonances at a set of wavelengths. In total six different structures with varying widths were prepared, as shown in Table 1. The periodicity p in different samples changes accordingly, such that the overall coverage ratio of each sample is roughly 50%. This ensures that the strengths of the magnetic resonances in different samples are comparable. The samples were fabricated by electron beam lithography (EBL) techniques. The geometries of the samples were first defined by use of an electron beam writer on a glass substrate with a thin layer of 15 nm indium-tin-oxide. Then standard electron beam deposition was used to produce a stack of silver and alumina layers corresponding to Fig. 1(a). Note that two thin alumina layers of 10 nm were added to the top and bottom of the Ag-Al_2O_3-Ag sandwich stacks for fabrication stability. The desired paired strips structures were obtained after a lift-off process. All six samples are on the same substrate and were fabricated simultaneously for a fair comparison. Each sample is 160 μm × 160 μm in size. Figures 1(b) and 1(c) show the field-emission scanning electron microscope (FE-SEM) and atomic force microscope (AFM) images of a typical paired nanostrip structure.

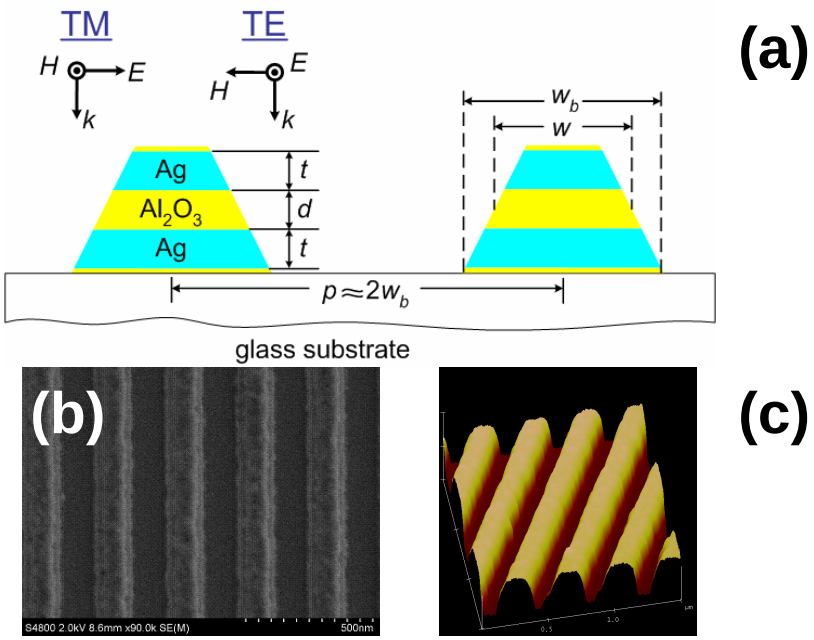

Fig. 1. Structure of the coupled nanostrip samples. (a) The cross-sectional schematic of arrays of coupled nanostrips; (b) The FE-SEM image of a typical sample; (c) The AFM image of a typical sample. Pictures in panels (b) and (c) correspond to sample E in Table 1.

Table 1. Geometric parameters of the magnetic nanostrip samples

Sample #	Bottom Width w_b	Average Width w	Periodicity p	Coverage % *
A	95	50	191	0.50
B	118	69	218	0.54
C	127	83	245	0.52
D	143	98	273	0.52
E	164	118	300	0.55
F	173	127	300	0.58

* Cover ratio is calculated by the ratio of bottom width w_b to the periodicity p.

#80062 - $15.00 USD
Received 13 February 2007; accepted 27 February 2007

3. Experimental characterizations

It has been demonstrated that nanostrip structures exhibit both magnetic and electric resonances under TM illumination with the magnetic field polarized along the strips (see Fig. 1(a) for polarization definition). For TE polarization with the electric field aligned with the strips, the structure has no resonant effects. To qualitatively illustrate the resonance properties of the magnetic samples with different strip widths, we took microscopic images of the samples for two orthogonal polarizations, as shown in Fig. 2. For the resonant TM polarization case [Figs. 2(a) and 2(c)], we observe distinct colors in different samples both in transmission mode and reflection mode indicating the different resonant frequencies in different samples. For the non-resonant TE polarization, however, the colors are the same for all samples. In this case the samples act as diluted metals with a behavior similar to perfect metals: more reflection and less transmission at longer wavelengths. This is why the non-resonant images appear blue in transmission mode [Fig. 2(b)] and red in reflection mode [Fig. 2(d)].

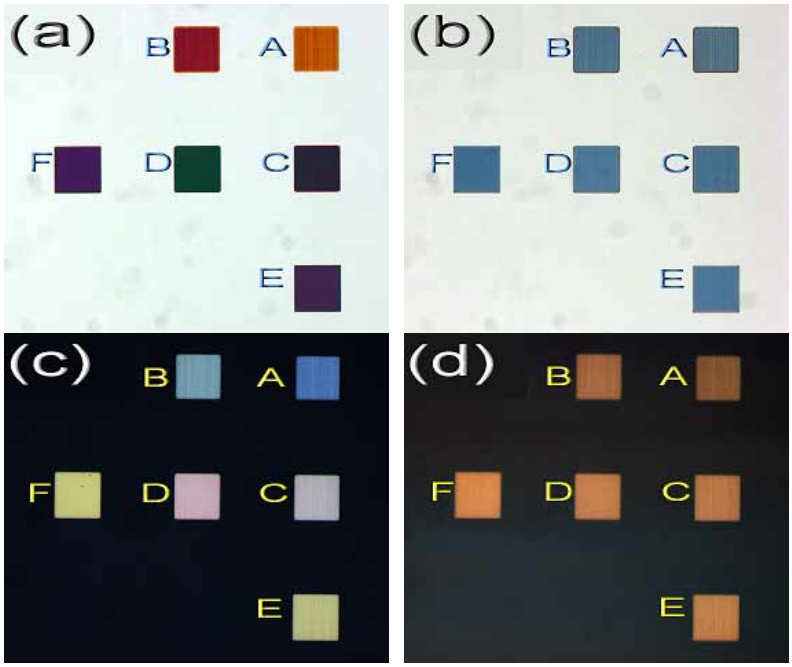

Fig. 2. Optical microscopy images of the magnetic samples for two orthogonal polarizations. (a) Transmission mode with TM polarization; (b) Transmission mode with TE polarization; (c) Reflection mode with TM polarization; (d) Reflection mode with TE polarization. Letters A-F correspond to the sample naming in Table 1.

In order to test samples with distinct resonance properties, we measured the transmission and reflection spectra of the nanostrip samples for both polarizations over a broad spectral range. The small sizes of the EBL-fabricated samples do not allow using a commercial spectrophotometer for spectral measurements. In this work we utilize an imaging approach with the setup shown in Fig. 3. The small sample with size S is imaged onto the focal plane of the collection system connected through a fiber bundle to a spectrograph. The magnified image size is $S\cdot(f_1/f_2)$, which is set to be significantly larger than the collecting area of optical system to ensure reliable data collection. Glan-Taylor prisms were placed at the output of the broadband lamps to select the light with the desired linear polarization. The transmission and reflection spectra were normalized to a bare substrate and a calibrated silver mirror, respectively.

#80062 - $15.00 USD Received 13 February 2007; accepted 27 February 2007

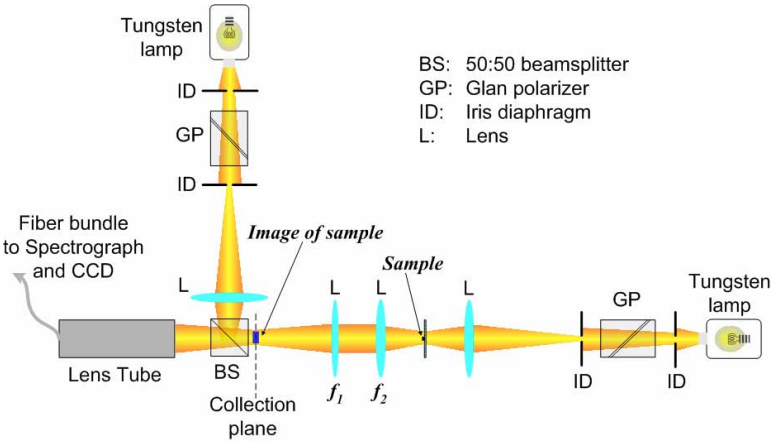

Fig.3. Experimental setup for collecting broadband transmission and reflection spectra of small samples.

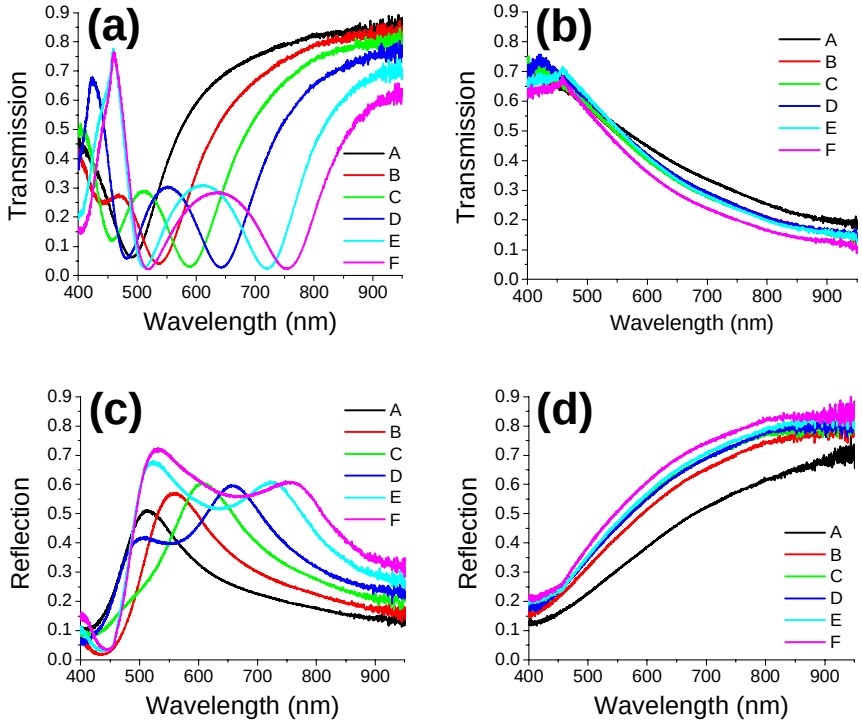

Fig 4. Transmission (T) and Reflection (R) spectra of the coupled nanostrip samples for two orthogonal polarizations. (a) T with TM polarization; (b) T with TE polarization; (c) R with TM polarization; (d) R with TE polarization. Letters A-F correspond to the sample naming in Table 1.

The collected spectra are shown in Fig. 4. As expected, we observe strong resonances from both transmission and reflection spectra for the TM polarization [Figs. 4(a) and 4(c)] For TE polarization, the spectra display a non-resonant wavelength dependence over a broad wavelength range [Figs. 4(b) and 4(d)]. The slopes of the spectra in TE mode confirm our claim regarding diluted metal and explain again why samples look blue in transmission mode [Fig. 2(b)] and red in reflection mode [Fig. 2(d)] for TE polarization. The six samples were

#80062 - $15.00 USD Received 13 February 2007; accepted 27 February 2007

fabricated with a range of strip widths from 50 nm (Sample A) to 127 nm (Sample F), and we obtained magnetic resonances occurring from 491 nm to 754 nm, covering the majority of the visible spectrum. The positions of the resonant wavelengths in TM mode move towards the blue when decreasing the width of the strips from Sample F to Sample A. This verifies the scaling property of the magnetic structure of coupled nanostrips.

The spectra for TM polarization exhibit important features at three distinct characteristic wavelengths. In Fig. 5 we plot the transmission, reflection and absorption (including diffractive scattering) spectra of a typical paired-strip sample (Sample E) under TM polarization with three characteristic wavelengths marked on the curves. The magnetic resonance around λ_m results from an anti-symmetric current flow in the upper and lower strips, which forms a circular current and gives rise to a magnetic dipole response [8]. This magnetic resonance is the major feature that we are pursuing in such a coupled nanostrip structure. In addition to the anti-symmetric current mode, the strip pair also supports a symmetric current mode at around λ_e, which results in an electric resonance. These two resonances induce the two local minima in the transmission spectra and local maxima in reflection, as illustrated in Fig. 5. The absorption spectrum in Fig. 5 shows enhanced absorption near the two resonance wavelengths λ_m and λ_e, which is natural for plasmonic resonances in metal-dielectric structures. The transmission spectrum also displays a sharp turn-back at a relatively short wavelength λ_d. This characteristic wavelength indicates the diffraction threshold and serves as a fingerprint of such grating-like structure. For a one dimensional grating with a periodicity p, a diffraction channel is created whenever the wavelength λ reaches below a diffraction threshold given by $\lambda_{d,j} = n_s p / j$, where j is an integer and n_s is the refractive index of the grating substrate (in our case, n_s = 1.52 for the glass substrate) [24]. When the wavelength λ falls below $\lambda_{d,j}$, strong distortion in the transmission is present and substantial optical power transfers to diffractive scattering, which is usually attributed to Wood's anomaly [25]. In our experiments this threshold is observed for Samples D, E and F, whose first-order threshold $\lambda_{d,1}$ is within the detection range of $\lambda > 400$ nm. The positions of $\lambda_{d,1}$ obtained from Fig. 4(a) for the three samples agree extremely well with calculated values, exhibiting deviations of less than 1%.

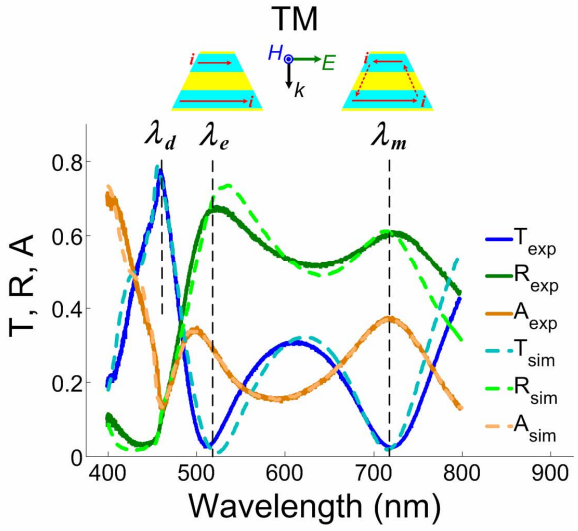

Fig. 5. Transmission (T) and Reflection (R) and absorption (A, including diffractive scattering) spectra under TM polarization for a typical coupled nanostrip sample (Sample E) with three characteristic wavelengths marked. Solid lines show the experimental data, and dashed lines represent simulated results. The two cross-sectional schematics of the strip-pair illustrate the current modes at electric and magnetic resonances, respectively.

#80062 - $15.00 USD Received 13 February 2007; accepted 27 February 2007

4. Simulations

In addition to experimental characterization, the properties of the coupled nanostrip samples were investigated by numerical simulations with a commercial finite element package. The material properties of silver are taken from well-accepted experimental data [26], with the imaginary part of the permittivity serving as an adjustable parameter to reflect the actual imperfection of the fabrication quality. A detailed description of the techniques used in simulating such structures were published elsewhere [14]. The transmission, reflection and absorption spectra for a representative sample (Sample E) are plotted in Fig. 5 along with the experimental data. All of the features observed in the experimental spectra are reproduced remarkably well in our numerical simulations.

To illustrate the nature of the magnetic and electric resonances, we simulation the field distribution at the two resonance wavelengths λ_m and λ_e of a representative coupled nanostrip sample obtained from a commercial finite element software (COMSOL Multiphysics), as shown in Fig. 6. The arrows represent the electric displacement whereas the color map represents the magnetic field. At the magnetic resonance [Fig. 6(b)] we note that the electric displacement forms a loop resulting in an artificial magnetic moment. We also note a strong magnetic field inside the loop. At the electric resonance [Fig. 6(a)] the electric displacement is predominantly aligned along one direction with a small circulating component. The magnetic field is also lower when compared to the magnetic resonance. The small circulating component of the electric displacement results in a small magnetic moment which manifests itself as the magnetic anti-resonance. The physics of the anti-resonance has been discussed extensively in Refs. [11], [14] and [27].

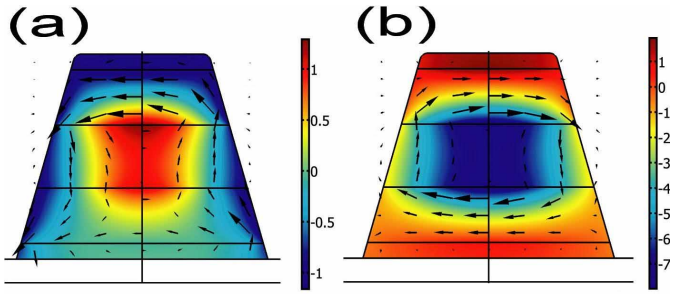

Fig. 6. Simulated electric displacement and magnetic field distributions at (a) the electric resonance λ_e and (b) the magnetic resonance λ_m.

5. Dependence of magnetic resonance on geometries

For practical designs and applications, it is desirable to have an analytical expression for the relation between the magnetic resonance wavelength λ_m and the geometric parameters (w, d, t) of the paired-strip structures. Following the cavity model approach discussed in Ref. [28], we find that for the range of parameters used in our experiments where $\lambda_m > 2n_d w$, the cavity resonant wavelengths λ_m are well described by

$$\varepsilon_m'(\lambda_m) = 1 - \frac{n_d^2}{t\kappa}\left[1 + \coth\left(\frac{d\kappa}{2}\right)\right], \quad \kappa = \sqrt{(\pi/w)^2 - \left(2\pi n_d/\lambda_m\right)^2}, \tag{1}$$

where ε_m' is the real part of the metal permittivity and n_d is the refractive index of the spacer. Because our fabricated structures are indeed more complicated than the ideal case described by the cavity model, there are small deviations between λ_m calculated with (1) and the experimentally observed values. Such deviations can be fully accounted by introducing in Eq. (1) the effective strip width w_{eff}. For the range of the used parameters, our calculations show that w_{eff} is only slightly smaller than the bottom width w_b of the coupled strips, namely $w_{eff} = 0.96 w_b$.

#80062 - $15.00 USD Received 13 February 2007; accepted 27 February 2007

Equation (1) has no analytical solution although it allows useful approximations in our case. We use the first-order approximations for the hyperbolic cotangent function in Eq. (1) with $d\kappa/2<<1$. In addition, we neglect the second term in the square root assuming $2n_d w<<\lambda_m$. The permittivity ε'_m of silver is approximated by the Drude model with $\varepsilon'_m(\lambda) = 5 - \lambda^2/\lambda_p^2$, where λ_p = 134.6 nm is the plasma wavelength of silver [26]. Then, we obtain the following approximate solution to Eq. (1):

$$\lambda_m = \sqrt{4 + \frac{n_d^2 w}{\pi t} + \frac{2n_d^2 w^2}{\pi^2 td}}\lambda_p. \qquad (2)$$

This approximation provides physical insight and confirms the intuitive conclusion that scaling down the width w of the strips results in a shorter resonant wavelength λ_m. Moreover, there is a less intuitive conclusion that reducing the thickness t of the metal strips tends to give λ_m a red-shift, which has been observed in our recent simulations and experiments [14]. Another interesting approximation for Eq. (1) can be obtained if the dimensions of coupled strips are relatively large ($w^2>>\lambda_p^2$ and $td>>\lambda_p^2$) whereas $d\kappa/2<<1$. In this case the resonant wavelength λ_m is independent of the thickness t and separation d, and it depends only on geometric parameter w: $\lambda_m \approx 2n_d w(1+\lambda_p^2/4\pi^2 td) \approx 2n_d w$. This limiting case describes well, for example, microwave magnetic media using paired metal wires [29], where the resonant wavelength is solely dependent on the length of the wires. Not surprisingly, the second approximation leads to a natural solution for the basic mode of an electromagnetic cavity with a characteristic size of w.

In Fig. 7 we plot the dependence of the magnetic resonance wavelength λ_m on the average width w of the trapezoidal-shaped paired strip samples both from experiments and analytical approaches. The experimental data for the relationship between λ_m and w is taken from Figs. 3(a) and 3(c). In Eq. (1), $w_{eff} = 0.96w_b$ is used for calculations. From Fig. 7 we can see that the results obtained from the Eq. (1) analytical method match the experimental data remarkably well. Therefore, the equations can be used as a general recipe for producing paired-strip magnetic metamaterials at any desired optical wavelength. Figure 7 also exhibits negligible saturation due to size scaling, which indicates that such a structure is capable of producing optical magnetism at even shorter wavelengths.

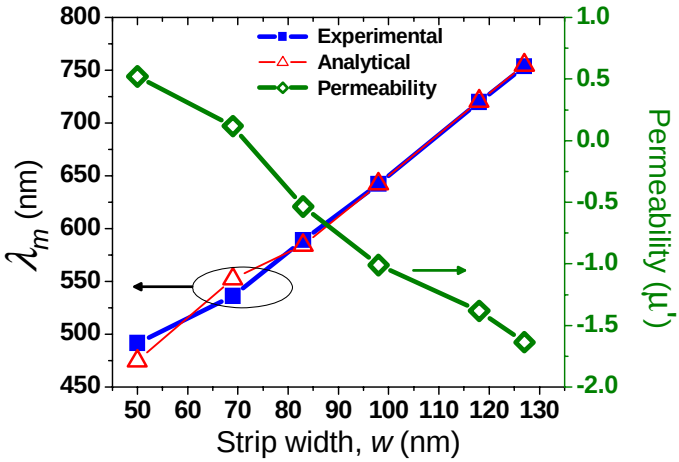

Fig.7. The dependence of the magnetic resonance wavelength λ_m on the average width w of the trapezoidal-shape paired strip samples, and the minimum values of permeability μ' for the six samples around λ_m. Square: experimental data for λ_m as a function of w from Figs. 4(a) and 4(c); Triangles: analytical $\lambda_m(w)$ relationship determined by Eq. (1); Diamond: retrieved minimum effective permeability for each sample.

#80062 - $15.00 USD Received 13 February 2007; accepted 27 February 2007

As for the strength of the magnetic responses in those samples, we retrieved the effective permeability μ' of each sample around the magnetic resonance wavelength λ_m using numerical simulations with the homogenization technique [9, 30]. For each sample, the material properties and geometrical parameters used in the retrieval procedure guarantee good agreement between the simulated and experimental broadband spectra. The minimum values of permeability for the six coupled-strip samples are shown in Fig. 7. The permeability obtained in each sample is distinct from unity, as opposed to conventional optical materials, and is found to be -1.6 in Sample F for dark-red light of 750 nm and 0.5 in Sample A at the blue wavelength of less than 500 nm. We note that for all the samples the magnetic resonance wavelength λ_m is at least five times larger than the strip width *w*, and therefore the coupled-strip samples can be regarded as two-dimensional metamaterials at the wavelengths of interest.

6. Conclusion

In summary, we have demonstrated a universal structure based on coupled nanostrips to create optical magnetic responses across the whole visible spectrum. The resonant properties of a family of such structures with varying dimensions were studied both experimentally and numerically. The obtained dependence of the magnetic resonance wavelength on the geometric parameters provides us with a general recipe for designing such magnetic metamaterials at any desired optical frequency. Additionally, it is possible to tune the magnitude of the effective permeability μ' by changing the coverage percentage of the stripes. Therefore, the coupled nanostrip structure can serve as a general building block for producing controllable optical magnetism for various practical implementations.

Acknowledgments

The authors would like to thank Jennie Sturgis of the Bindley Bioscience Center at Purdue University for her gracious help with optical microscopy images. This work was supported in part by ARO grant W911NF-04-1-0350, ARO-MURI award 50342-PH-MUR, and NSF-PREM Grant #DMR-0611430.

#80062 - $15.00 USD Received 13 February 2007; accepted 27 February 2007